Oscillatory Peroxodisulfate Reduction on Pt and Au Electrodes under High Ionic Strength Conditions, Caused by the Catalytic Effect of Adsorbed OH

Shuji Nakanishi, Sho-ichiro Sakai, Michiru Hatou, Yoshiharu Mukouyama, and Yoshihiro Nakato*

Department of Chemistry, Graduate School of Engineering Science, Osaka University, and Research Center for Solar Energy Chemistry, Osaka University, Toyonaka, Osaka 560-8531, Japan

Received: August 24, 2001; In Final Form: November 29, 2001

Four electrochemical oscillations of different types (named oscillations α, *β*, *γ*, and *δ*), which are different from previously reported Frumkin-type oscillations in low ionic strength electrolytes, appear for peroxodisulfate ($S_2O_8^{2-}$) reduction on Pt and Au electrodes under high ionic strength conditions. Impedance measurements for oscillation *γ* that appears in a region of the most positive potentials have shown that it is classified as hidden negative differential resistance (hidden-NDR or HNDR) oscillators. Detailed electrochemical measurements have suggested that the NDR arises from a decrease (with a negative potential shift) in the surface coverage of adsorbed OH, which acts as a catalyst for the dissociative adsorption of $S_2O_8^{2-}$ (the first step of its reduction). The NDR is hidden by the desorption (with the negative potential shift) of adsorbed sulfate (SO_4^{2-}) produced by the dissociative adsorption and reduction of $S_2O_8^{2-}$, which works as a site-blocking agent. Mathematical simulation based on this model has reproduced the appearance of oscillation *γ*. The result supports our previously proposed concept of autocatalytic effect of adsorbed OH and catalytic effect of adsorbed halogen on the dissociative adsorption of H_2O_2, showing the generality of the electrocatalytic effect of adsorbed OH and halogen.

Introduction

Electrochemical reactions with nonlinear kinetics show a variety of interesting dynamic behavior such as periodic and chaotic oscillations.[1−4] Mechanistic studies of electrochemical oscillations have made rapid progress recently, resulting in classification on the basis of the oscillation mechanisms.[4,5] Very recently, growing attention has been paid to the observation and understanding of spatiotemporal patterns arising from nonlinear kinetics, such as traveling chemical waves[6−10] and Turing patterns.[11]

We have reported thus far[12−19] that H_2O_2 reduction on Pt electrodes in acidic solution shows at least five oscillations of different types, depending on the electrode potential and the current density, the atomic level flatness of the electrode surface, and the presence or absence of halogen ions in solution. The finding of such new oscillations led to the improvement of the classification of electrochemical oscillations.[15,16] Moreover, the studies have revealed new mechanisms for electrochemical reactions themselves, such as an autocatalytic effect of adsorbed OH on the dissociative adsorption of H_2O_2[12,17] and a catalytic effect of adsorbed halogen on the same reaction,[16,19] which will be important not only for oscillation studies but also for exploration of new active electrode materials for fuel cells. A similar autocatalytic effect of adsorbed OH is reported for an oscillation in H_2O_2 reduction on Ag electrodes.[20]

Unfortunately, modern atomic level techniques for further confirmation of the above new mechanisms, such as electrochemical quartz crystal microbalance (EQCM) and FTIR techniques, are difficult to apply to adsorbed OH that is the key intermediate of the H_2O_2 reduction. Thus, we started studies on electrochemical oscillations in $S_2O_8^{2-}$ reduction, to which the EQCM and FTIR techniques will be applicable because of the large mass of adsorbed $S_2O_8^{2-}$ and SO_4^{2-} and strong IR absorption of adsorbed SO_4^{2-} at 1100−1200 cm^{-1}. The purpose of this paper is to find an oscillation mechanism in the $S_2O_8^{2-}$-reduction system, similar to that found in the H_2O_2-reduction system, which enables to use the above atomic level techniques for the further confirmation of the mechanism.

The electrochemical oscillation in the $S_2O_8^{2-}$ reduction was first reported by Frumkin et al.,[21] and since then, a lot of investigations have been done on this system.[22−27] However, most studies have been made using electrolytes of low ionic strength, in which the origin of the oscillations (or the negative differential resistances) comes from the electrostatic repulsion of a negatively charged electrode to electroactive anions, $S_2O_8^{2-}$ (so-called the Frumkin effect). In this work, we used electrolytes of high ionic strength, in which the Frumkin effect is neglected, and found that the $S_2O_8^{2-}$ reduction on Pt or Au electrodes shows four oscillations of different types (named oscillations α, *β*, *γ*, and *δ*). Detailed studies have revealed that oscillation *γ*, appearing in the most positive potentials, arises from the catalytic effect of adsorbed OH on the dissociative adsorption of $S_2O_8^{2-}$, similarly to oscillations C and E in the H_2O_2-reduction system.

Experimental Section

Polycrystalline Pt (99.9% in purity) and Au (99.99%) disks of about 6.0 mm in diameter and single-crystal Au (99.999%) disks of about 2−3 mm in diameter were used as the working electrode. The poly-Pt and Au disks were polished with 0.06 *μ*m alumina slurry and immersed in a hot (HNO_3 + H_2O_2) solution for 10 min to remove surface contamination. Just before

* Corresponding author. Tel: +81-6-6850-6235. Fax: +81-6-6850-6236. E-mail: nakato@chem.es.osaka-u.ac.jp.

10.1021/jp013275p CCC: $22.00
Published on Web 02/09/2002

measurements, cyclic potential scans were repeated between −0.50 and +1.50 V vs SCE in 0.5 M $HClO_4$ (M = mol/dm^3) for about 30 min for further cleaning of the electrode surface. Single-crystal Au(111), -(100), and -(110) electrodes with atomically flat surfaces were prepared by the method of Clavilier et al.[28] The details of the preparation method were described in a previous paper.[17]

Current density (j) vs potential (U) curves and j vs time (t) curves were measured with a potentiogalvanostat (Nikko-Keisoku, NPGS-301) and a potential programmer (Nikko-Keisoku NPS-2), using a Pt plate (10 × 10 mm^2) as the counter electrode and a saturated calomel electrode (SCE) as the reference electrode. The data were recorded with an X−Y recorder (Riken-Denshi F-35C) or a data-storing system (instruNET, GW Instruments) with a sampling frequency of 1 kHz. The electrolyte solutions were prepared using special grade chemicals and pure water, the latter of which was obtained by purification of deionized water with a Milli-Q water purification system. The electrolyte solutions were kept stagnant during measurements. The ohmic drops in the solution between the working electrode and the reference electrode were not corrected in this work.

Impedance measurements were carried out with a Solartron 1260 impedance analyzer combined with a Solartron 1287 electrochemical interface potentiostat. The amplitude of modulation potential was 10 mV. Just before the measurements, the electrode potential was held at a potential at which the measurement was done, for about 180 s, to accomplish a steady distribution of the $S_2O_8^{2-}$ concentration.

Results

Figures 1 and 2 summarize four electrochemical oscillations, named oscillations α, β, γ, and δ, observed for the $S_2O_8^{2-}$ reduction on poly-Au (Figure 1) and poly-Pt (Figure 2) electrodes. Figure 3 summarizes, for reference in later discussion, reported oscillations for the H_2O_2 reduction on Pt.[15,17]

Figure 1a shows a $j-U$ curve for poly-Au in 0.5 M $HClO_4$ without $S_2O_8^{2-}$, which is included to show the potential region of formation and disappearance of surface Au oxide. No current peaks corresponding to hydrogen adsorption and desorption are observed for Au, contrary to the case of Pt (cf. Figure 2a). When 0.5 M $Na_2S_2O_8$ is added to the solution (Figure 1b), a cathodic current due to the $S_2O_8^{2-}$ reduction starts at about 0.4 V vs SCE, just a potential at which the reduction of surface Au oxide is nearly completed (Figure 1a). According to the work by Müller et al.[29,30] and Samec et al.[26,31] using rotating Au electrodes, $S_2O_8^{2-}$ reduction on Au proceeds via two pathways. The first one is initiated by the dissociative adsorption of $S_2O_8^{2-}$, probably followed by immediate reduction of adsorbed $SO_4^{\bullet-}$ radicals,

$$S_2O_8^{2-} \rightarrow 2SO_4^{\bullet-}{}_{ad} \qquad (1a)$$

$$SO_4^{\bullet-}{}_{ad} + e^- \rightarrow SO_4^{2-}{}_{ad} \qquad (1b)$$

This pathway gives a current near the onset of the $S_2O_8^{2-}$ reduction in a region from +0.4 to 0 V (see Figure 1b). The other pathway is a direct reduction of $S_2O_8^{2-}$ via no adsorption,

$$S_2O_8^{2-}{}_{aq} + e^- \rightarrow SO_4^{\bullet-}{}_{aq} + SO_4^{2-}{}_{aq} \qquad (2a)$$

$$SO_4^{\bullet-}{}_{aq} + e^- \rightarrow SO_4^{2-}{}_{aq} \qquad (2b)$$

and the corresponding current is observed in a region of more negative potentials from 0 to −0.6 V or further negative potentials. Hydrogen evolution starts at about −0.8 V in Figure 1b.

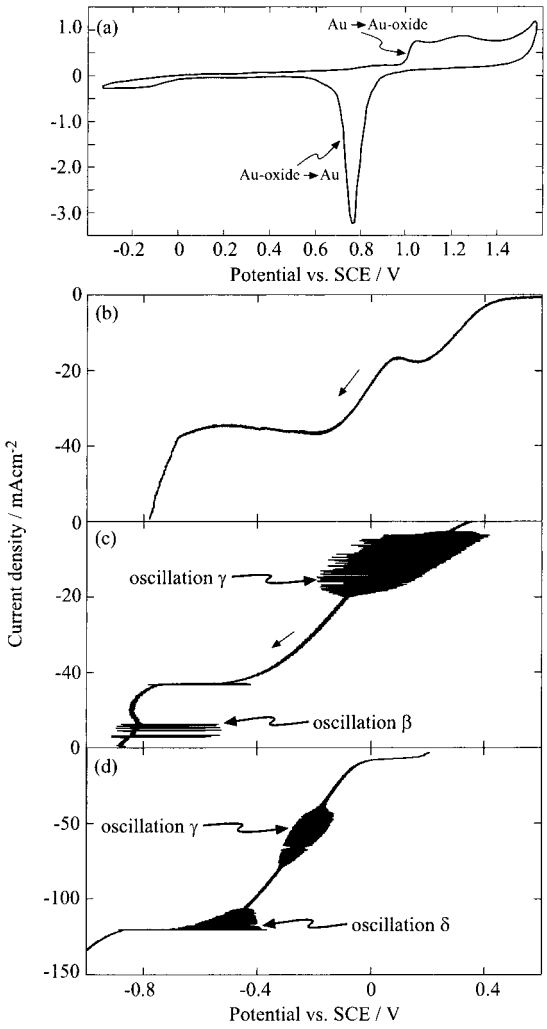

Figure 1. Current density (j) vs potential (U) curves for poly-Au under (a, b) potential-controlled and (c, d) current-controlled conditions. Electrolyte: (a) 0.5 M $HClO_4$; (b−d) 0.5 M $HClO_4$ + 0.5 M $Na_2S_2O_8$. Scan rate: (a) 100 mV/s; (b) 10 mV/s; (c) 1 mA/s; (d) 10 mA/s.

Under current-controlled conditions for Au electrodes, three oscillations (oscillations β, γ, and δ) appear, as shown in Figure 1c,d. It is to be noted that oscillation γ appears in a region of the most positive potentials, i.e., in a potential region of reaction 1. On the other hand, oscillation β appears in a potential region of reaction 2 and hydrogen evolution, similarly to oscillation B in the H_2O_2-reduction system which also appears in a region of hydrogen evolution (Figure 3).[12,13,16] Zelin et al.[32] reported an oscillation for the $S_2O_8^{2-}$ reduction on Ag in 1.0 M NaOH, which may correspond to oscillation β in the present work. Oscillation δ appears between oscillations γ and β when the scan rate of j is made rapid (Figure 1d). Oscillation δ was unstable under a constant current density and weakened in amplitude with time, finally disappearing.

Figure 2 shows $j-U$ curves for poly-Pt. When 0.7 M $S_2O_8^{2-}$ is added (Figure 2b), the $S_2O_8^{2-}$-reduction current starts at about 0.2 V, at which the reduction of surface Pt oxide is nearly completed (Figure 2a), and increases (in the absolute value) with the decreasing potential, in a manner similar to the case of Au electrodes. (Note that the current peaks in Figure 2a are not observed in Figure 2b owing to a large difference in the current-density scale.) Hydrogen evolution starts at about −0.4 V, and in a narrow potential region just before it, oscillation α appears

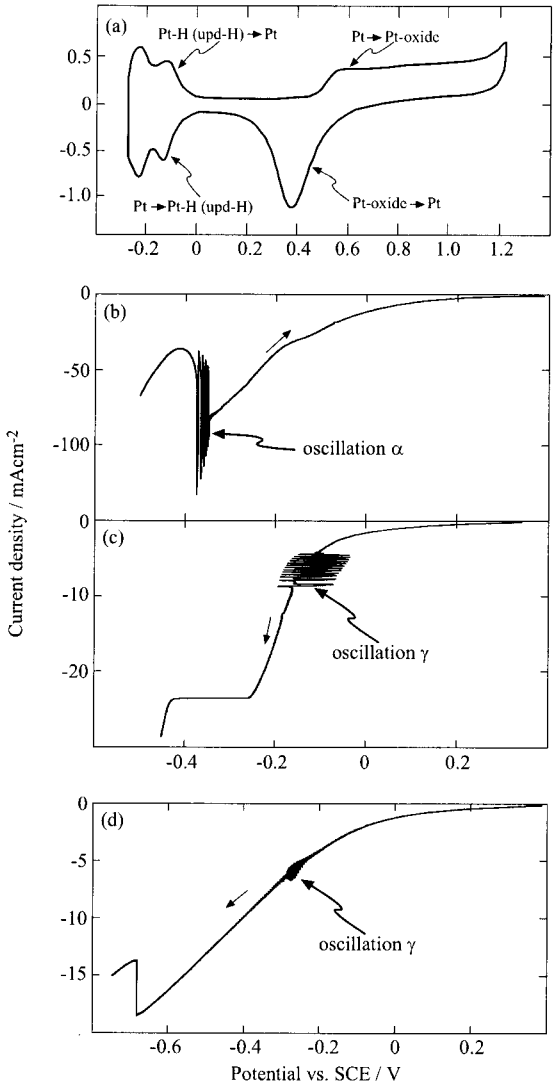

Figure 2. $j-U$ curves for poly-Pt under (a), (b), and (d) potential-controlled and (c) current-controlled conditions. Electrolyte: (a) 0.5 M $HClO_4$; (b) 0.5 M $HClO_4$ + 0.7 M $Na_2S_2O_8$; (c, d) 0.5 M $HClO_4$ + 0.5 M $Na_2S_2O_8$. Scan rate: (a) 100 mV/s; (b, d) 10 mV/s; (c) 1 mA/s. An external resistance of 120 Ω is added for (d).

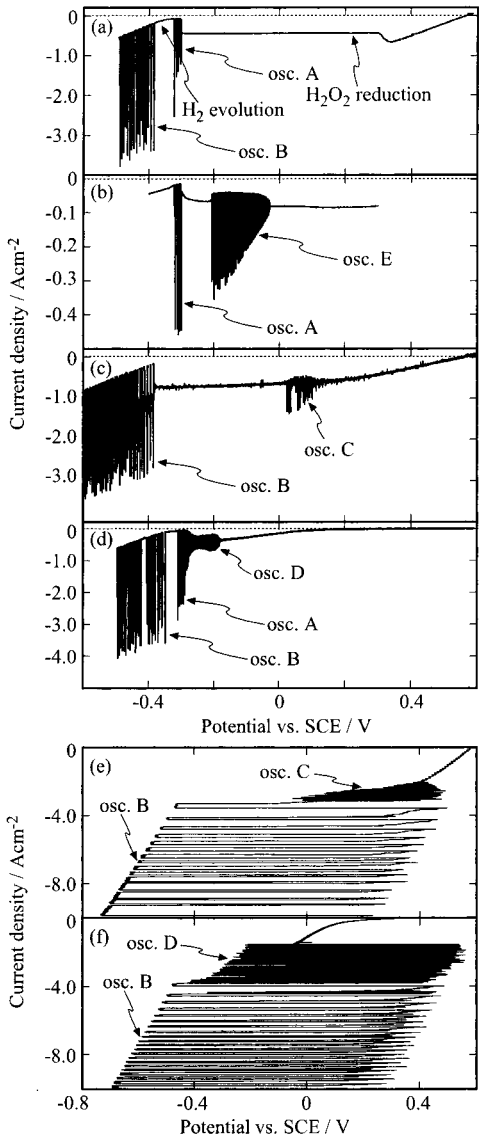

Figure 3. Reported five oscillations, called oscillation A−E, observed for the H_2O_2 reduction on Pt in an acidic solution under (a−d) potential-controlled and (e, f) current-controlled conditions. Electrode: poly-Pt except that single-crystal Pt(111) is used for (b). Oscillation E is observed only for Pt(111). Electrolyte: 0.3 M H_2SO_4 containing (a) 0.7 M H_2O_2, (b) 1.0 M H_2O_2, (c, e) 1.2 M H_2O_2 + 1.0×10^{-3} M KCl, and (d, f) 0.7 M H_2O_2 + 1.0×10^{-4} M KBr.

(Figure 2b). This behavior of oscillation α is the same as that of oscillation A in the H_2O_2-reduction system (Figure 3). We reported previously[12,13] that oscillation A arises from an NDR due to the suppression of the H_2O_2 reduction by the formation of upd-H (underpotential-deposited hydrogen) of a nearly full coverage. Oscillation α in Figure 2b may thus appear by the same mechanism as oscillation A, a slight negative shift of the potential region of oscillation α from that of the upd-H in Figure 2a being attributed to the ohmic drop in solution. This explanation is supported by the fact that oscillation α appears only for Pt electrodes on which upd-H is formed and not for Au.

Under current-controlled conditions for Pt electrodes, oscillation γ is observed, similar to the case of Au, though oscillations β and δ are not observed. Oscillation γ for Pt appears in the most positive potentials. In addition, oscillation γ appears under potential-controlled conditions if an external resistance of about 120 Ω is added (Figure 2d). We can thus say that oscillation γ is of a character similar to oscillation C in the H_2O_2-reduction system, which is also observed under both current- and potential-controlled conditions in a region of the most positive potentials (Figure 3).

We made detailed studies on oscillation γ because it appears initially and thus its mechanism may be understood most easily. Figure 4 shows a waveform of oscillation γ as a potential oscillation at -10 mA cm^{-2} in 0.7 M $Na_2S_2O_8$ + 0.5 M $HClO_4$. The stable and periodic oscillation continued for about 10 min or more. Figure 5 shows an impedance diagram for poly-Au in 0.7 M $Na_2S_2O_8$ + 0.5 M $HClO_4$ at -0.16 V vs SCE, near which oscillation γ appears (Figure 1c). The diagram clearly shows the presence of an HNDR (i.e., negative differential resistances in a region of intermediate frequencies and positive differential resistances in low frequencies), indicating that oscillation γ is an HNDR oscillator. Oscillation C is also classified into HNDR oscillators.[15]

In accordance with the above result, the $j-U$ curves under potential-controlled conditions, measured at a high scan rate of 100 mV/s, showed an NDR in a region of 0.2−0.0 V (Figure 6), though the NDR is not clear at a low scan rate (Figure 1b). The NDR at a high scan rate was observed prominently for

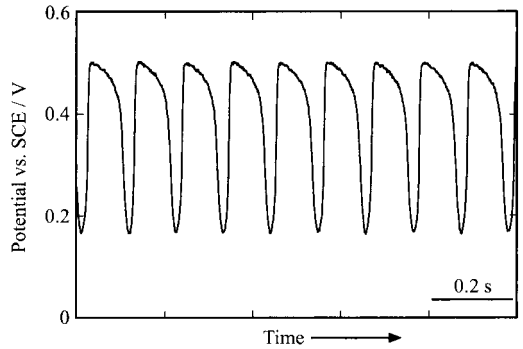

Figure 4. Potential (U) vs time (t) curve at -10 mA cm^{-2} for poly-Au in 0.5 M $HClO_4$ + 0.7 M $Na_2S_2O_8$.

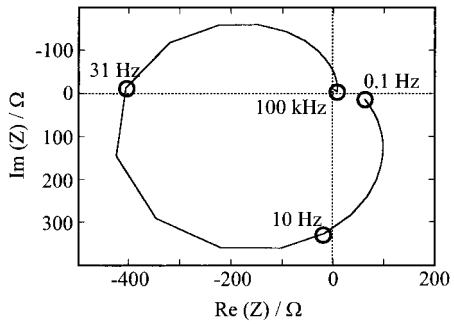

Figure 5. Impedance diagram for poly-Au at -0.16 V vs SCE in 0.5 M $HClO_4$ + 0.7 M $Na_2S_2O_8$.

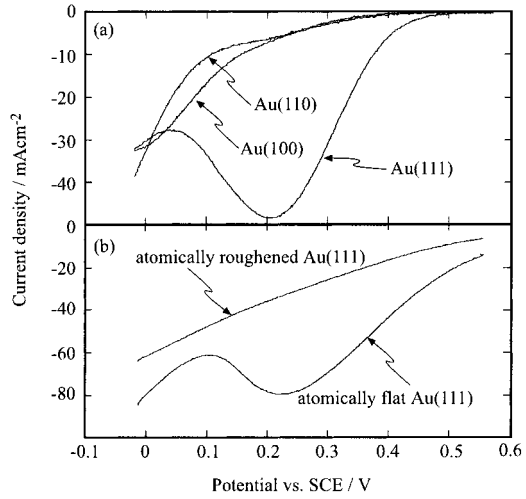

Figure 6. Dependences of the $j-U$ curves on (a) the crystal faces and (b) the surface atomic flatness for single-crystal Au electrodes under potential-controlled conditions. Electrolyte: 0.5 M $HClO_4$ + 0.7 M $Na_2S_2O_8$. The scan rate is 100 mV/s.

atomically flat Au(111) but not for Au(100) and Au(110) (Figure 6a). The atomically roughened Au(111), prepared by repeated electrochemical oxidation and rereduction,[17,33] also showed no NDR (Figure 6b). Quite the same behavior was observed for the NDR in the H_2O_2-reduction system, from which oscillation C as well as oscillation E appears. Namely, the NDR in the H_2O_2-reduction system, originating from an autocatalytic effect of adsorbed OH on the dissociative adsorption of H_2O_2, was prominent for atomically flat Pt(111) but not for Pt(100) and Pt(110) and atomically roughened Pt(111).[17] This fact strongly suggests that the NDR in Figure 6 appears by a mechanism similar to that for the above NDR in the H_2O_2-reduction system, or in other words, oscillation γ appears by a mechanism similar

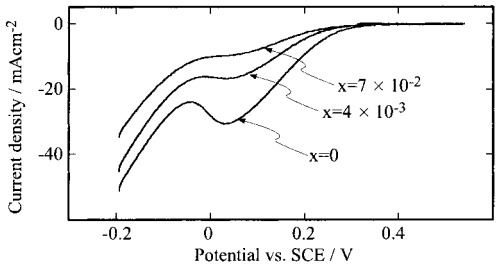

Figure 7. Effect of addition of SO_4^{2-} to the solution on the $j-U$ curves for poly-Au under potential-controlled conditions. Electrolyte: 0.5 M $HClO_4$ + 0.7 M $Na_2S_2O_8$ + x M Na_2SO_4, where x is indicated in the figure. The scan rate is 100 mV/s.

to that for oscillation C. Why the NDR is observed only at high scan rates and for atomically flat Au(111) (Figure 6) will be explained in the next section.

Oscillation γ is classified into an HNDR oscillator, as mentioned earlier (Figure 5). To clarify what is the NDR-hiding species, we investigated the effect of addition of SO_4^{2-} ions to the solution, which are a product of the $S_2O_8^{2-}$ reduction (reaction 1). Figure 7 shows that the NDR, observed in $+0.05$ to -0.05 V in the absence of SO_4^{2-}, is gradually hidden with the increasing concentrations of added SO_4^{2-}, accompanied by a decrease in the $S_2O_8^{2-}$-reduction current, which strongly suggests that adsorbed SO_4^{2-} is an NDR-hiding species.

Mathematical Simulation

The experimental results indicate that (1) oscillation γ appears in a potential region where the $S_2O_8^{2-}$ reduction proceeds via its dissociative adsorption (reaction 1), (2) oscillation γ is an HNDR oscillator, (3) the NDR is likely to arise form a catalytic effect of adsorbed OH on the dissociative adsorption of $S_2O_8^{2-}$, and (4) the NDR-hiding species is most probably adsorbed SO_4^{2-} produced by reaction 1. Thus, there is a good parallelism between oscillation γ and previously reported oscillation C, which also appeared from the NDR due to the autocatalytic effect of adsorbed OH on the dissociative adsorption of H_2O_2, with adsorbed halogen as the NDR-hiding species.

The observation of the NDR for oscillation γ only at high scan rates and for atomically flat Au(111) (Figure 6) can be explained, on the basis of the reported mechanism[15,17] in the H_2O_2 reduction system, as follows: First, the surface coverage (θ_{OH}) of adsorbed OH, acting as a catalyst for reaction 1a, decreases with a negative potential scan, which leads to a decrease in the $S_2O_8^{2-}$-reduction current with the negative potential scan, i.e., the appearance of an NDR. The observation of the NDR only at high scan rates (or the disappearance of the NDR at low scan rates) can be attributed to *slow* desorption of adsorbed SO_4^{2-} produced by reaction 1. Namely, at low scan rates, the decrease in the amount of adsorbed OH due to the decrease in θ_{OH} is compensated by an increase in empty surface sites by desorption of adsorbed SO_4^{2-}. The observation of the NDR only for flat Au(111) can be attributed to the effective autocatalytic effect of adsorbed OH on this face,[17,19] as explained in more detail later (Figure 10).

We created a mathematical simulation for oscillation γ on the basis of the above model. We took into account the catalytic effect of adsorbed OH on reaction 1a by expressing the rate constant k_{1a} as follows:

$$k_{1a} = k_{1a0} + \zeta\theta_{OH} \tag{3}$$

Here k_{1a0} is a normal rate constant and ζ is a proportional constant. The following reactions were considered in addition

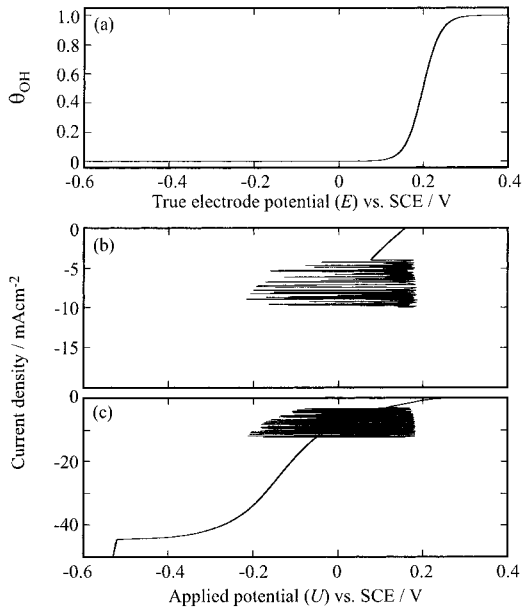

Figure 8. (a) θ_{OH} vs E, calculated by eq 12, with $a = 45\ V^{-1}$ and $E_{50}' = +0.2$ V vs SCE. (b) j vs U calculated by eqs 7−12 with $k_{1a0} = 4.5 \times 10^{-3}$ cm s^{-1}, $\zeta = 5$, and a scan rate of 2 mA/s, under the condition that the calculation is carried out within a range of j from 0 to −10 mA cm^{-2}. (c) Improved j vs U calculated by adding contributions of reaction 2 and hydrogen evolution. Other parameter values are $C_{SO}^{b} = 0.7 \times 10^{-3}$ mol cm^{-3}, $\delta = 0.015$ cm, $D = 5.0 \times 10^{-6}$ cm^2 s^{-1}, $A = 0.28$ cm^2, $C_{DL} = 2.0 \times 10^{-5}$ F cm^{-2}, $N_0 = 2.2 \times 10^{-9}$ mol cm^{-2}, $R_\Omega = 10\ \Omega$, $T = 300$ K, $\alpha_i = 0.25$ for $i =$ 1b and 4 and 0.50 for others, $n = 1$, $k_{1b0} = 6.5 \times 10^{-4}$ mol cm^{-2} s^{-1}, $E_{1b0} = 1.0$ V vs SCE, $k_{20} = 1.0 \times 10^{-8}$ cm s^{-1}, $E_{20} = 0.4$ V, $k_{40} = 3.0 \times 10^{-9}$ mol cm^{-2} s^{-1}, and $E_{40} = 0.5$ V.

to the aforementioned reactions 1a,b:

$$SO_4^{2-}{}_{ad} \rightarrow SO_4^{2-}{}_{aq} \quad (4)$$

$$OH_{ad} + H^+ + e^- \leftrightarrow H_2O \quad \text{(in the presence of } S_2O_8^{2-}) \quad (5)$$

The rate constant for electrochemical reaction i, k_i, was given by the Butler−Volmer equation with the conventional notations:[12,14]

$$k_i = k_{i0} \exp[-\alpha n F(E - E_{i0})/RT] \quad (6)$$

The differential equations for a current balance, mass balances, and rate equations were given in the same way as in previous work,[12,14−19]

$$I = jA = (U - E)/R_\Omega = I_C + I_F = AC_{DL}(dE/dt) + I_F \quad (7)$$

$$I_F = AF(-k_{1b}\theta_1) \quad (8)$$

$$(\delta/2)\, dC_{SO}^{s}/dt = (D/\delta)(C_{SO}^{b} - C_{SO}^{s}) - k_{1a}C_{SO}^{s}(1 - \theta_1 - \theta_2 - \theta_{OH})^2 \quad (9)$$

$$N_0\, d\theta_1/dt = 2k_{1a}C_{SO}^{s}(1 - \theta_1 - \theta_2 - \theta_{OH})^2 - k_{1b}\theta_1 \quad (10)$$

$$N_0\, d\theta_2/dt = k_{1b}\theta_1 - k_4\theta_2 \quad (11)$$

where θ_1 and θ_2 are the surface coverages of adsorbed $SO_4^{\bullet-}$ and SO_4^{2-}, respectively, and C_{SO}^{s} and C_{SO}^{b} the concentrations of $S_2O_8^{2-}$ at the electrode surface and in the solution bulk, respectively. D is the diffusion coefficient for $S_2O_8^{2-}$, δ the thickness of a diffusion layer for $S_2O_8^{2-}$, and N_0 the total amount of surface sites/unit area.

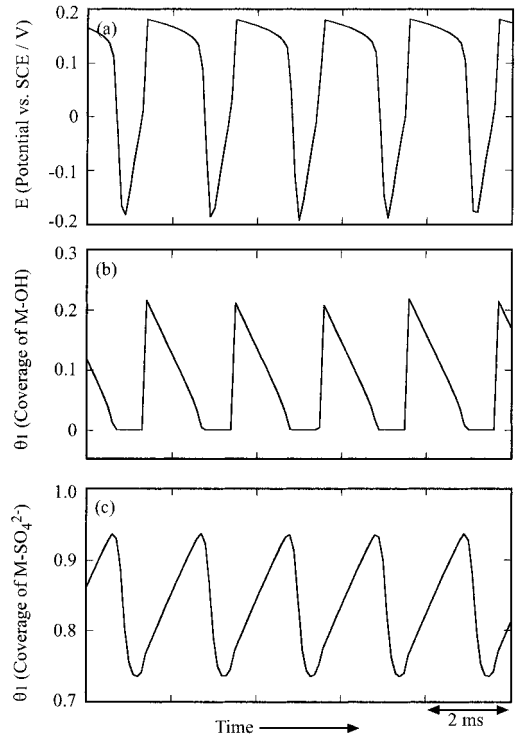

Figure 9. Calculated $E-t$, θ_1-t, and θ_2-t curves at $j = -10$ mA cm^{-2}. The parameter values are the same as in Figure 8.

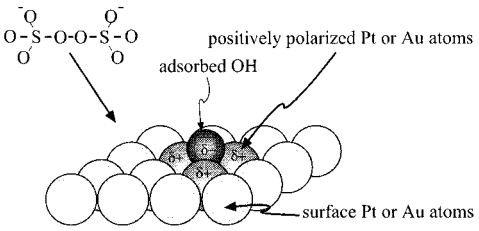

Figure 10. Schematic illustration of a catalytic effect of adsorbed OH for the dissociative adsorption of $S_2O_8^{2-}$.

The site-blocking effect of adsorbed SO_4^{2-} (slow species), together with those of adsorbed $SO_4^{\bullet-}$ and OH, was taken into account by introducing such terms as $(1 - \theta_1 - \theta_2 - \theta_{OH})$ in the rate equations. The rate of reaction 5 was not explicitly considered in eq 8, because reaction 5 is actually a complex reaction, affected by a certain action of $S_2O_8^{2-}$ ions (as discussed later). The calculation of $j-U$ curves with the neglect of reaction 5 reproduced well the observed curves, as mentioned later, indicating that reaction 5 makes no substantial contribution to the current.

The θ_{OH} vs E relation can be expressed, if we can assume that reaction 5 is in equilibrium at every (true) electrode potential (E), in the form[12]

$$\theta_{OH} = 1/[1 + \exp\{-a(E - E_{50}')\}] \quad (12)$$

where a equals (RT/nF) and E_{50}' refers to the apparent equilibrium potential for reaction 5 in the presence of $S_2O_8^{2-}$. E_{50}' will be somewhat more negative than the (true) equilibrium potential, E_{50}, for reaction 5 in the absence of $S_2O_8^{2-}$. In the present work, E_{50}' was estimated from the reported experiment[34] discussed later and a was taken as a parameter. Figure 8a shows a θ_{OH} vs E relation calculated with $a = 45\ V^{-1}$ and $E_{50}' =$

+0.2 V vs SCE. The θ_{OH} changes from nearly one to nearly zero in a range of E from about 0.3 to 0.1 V.

Figure 8b shows a $j-U$ curve calculated by use of eqs 7−12 under the condition that the calculation is carried out within a range of j from zero to −10 mA cm^{-2}. The curve reproduces the appearance of oscillation γ as a potential oscillation. If the above condition is removed, computers cannot finish calculations, not giving any $j-U$ curves, because reactions 1, 4, and 5 cannot give current densities higher (in the absolute value) than about 10 mA cm^{-2}. This is because, at more negative potentials than the calculated potential region in Figure 8b, θ_{OH} approaches zero and k_{1a} becomes quite small ($k_{1a} \approx k_{1a0}$), leading to small j.

Figure 8c shows an improved $j-U$ curve obtained by adding contributions of reaction 2, the second pathway for the $S_2O_8^{2-}$ reduction, and hydrogen evolution.

$$H^+ + e^- \leftrightarrow H_{ad} \quad (13)$$

$$2H_{ad} \rightarrow H_2 \quad (14)$$

In this case, eqs 8−10 are modified as follows, together with the addition of another differential eq 15 for the coverage (θ_H) of adsorbed hydrogen,

$$I_F = AF\{-k_{1b}\theta_1 - 2k_2 C_{SO}{}^s (1 - \theta_1 - \theta_2 - \theta_{OH} - \theta_H) - k_{13} C_H{}^s (1 - \theta_1 - \theta_2 - \theta_{OH} - \theta_H) + k_{-13}\theta_H\} \quad (8')$$

$$(\delta/2)\, dC_{SO}{}^s/dt = (D/\delta)(C_{SO}{}^b - C_{SO}{}^s) - k_{1a} C_{SO}{}^s (1 - \theta_1 - \theta_2 - \theta_{OH} - \theta_H)^2 - k_2 C_{SO}{}^s (1 - \theta_1 - \theta_2 - \theta_{OH} - \theta_H) \quad (9')$$

$$N_0\, d\theta_1/dt = 2k_{1a} C_{SO}{}^s (1 - \theta_1 - \theta_2 - \theta_{OH} - \theta_H)^2 - k_{1b}\theta_1 \quad (10')$$

$$N_0\, d\theta_H/dt = k_{13} C_H{}^s (1 - \theta_1 - \theta_2 - \theta_{OH} - \theta_H) - k_{-13}\theta_H - 2k_{14}\theta_H{}^2 \quad (15)$$

where k_{13} and k_{-13} are the rate constants for the forward and backward processes of reaction 13, respectively, and $C_H{}^s$ is the surface concentration of H^+ ions. The $j-U$ curve in Figure 8c is in good agreement with the observed curves (Figures 1c and 2c), except the appearance of oscillation β. Figure 9 shows a calculated $E-t$ curve at a constant current density of −10 mA cm^{-2}, together with θ_1-t and θ_2-t curves. The calculated $E-t$ reproduces the essential feature of the waveform of oscillation γ as a potential oscillation (Figure 4).

Discussion

The experimental results and mathematical simulation have shown that oscillation γ is an HNDR oscillator and the NDR arises from the catalytic effect of adsorbed OH on the dissociative adsorption of $S_2O_8^{2-}$. Here arises a question whether the adsorbed OH can exist even in a potential region of oscillation γ, which is considerably more negative than the current peak for the reduction of surface Au or Pt oxide (Figures 1a and 2a). It is reported by surface-enhanced Raman spectroscopy (SERS)[34] that, in the presence of 1−20 mM $S_2O_8^{2-}$, oxygen-containing adsorbed species (most probably attributable to adsorbed OH) survive on Au down to potentials 0.3−0.4 V more negative than the reduction peak of surface oxide. The strong oxidant, $S_2O_8^{2-}$, is likely to induce chemical (or electrochemical) oxidation of the Au surface leading to formation of adsorbed OH, though the detailed mechanism is unknown.

The effect of addition of SO_4^{2-} ions to the solution (Figure 7) shows that adsorbed SO_4^{2-} acts as the NDR-hiding species. Oscillation γ appears without any addition of SO_4^{2-}, because adsorbed SO_4^{2-}, produced by the $S_2O_8^{2-}$ reduction (reaction 1b), can act as the NDR-hiding species, as mentioned before. This is an interesting example, for, in most cases, adsorbed species as the NDR-hiding species are supplied by the adsorption of solution species added.[5]

On the basis of the results of mathematical simulation (Figures 8 and 9), oscillation γ can be explained as follows. In a high-potential state of a potential oscillation at a constant current density, the surface coverage of adsorbed OH (θ_{OH}) is large and, thus, $k_{1a} \gg k_{1a0}$; i.e., the $S_2O_8^{2-}$ reduction occurs efficiently, which leads to an increase in the coverage (θ_2) of adsorbed SO_4^{2-} as a product of the $S_2O_8^{2-}$ reduction owing to slow desorption of adsorbed SO_4^{2-} (slow species). The increase in θ_2 leads to a decrease in vacant surface sites at which the dissociative adsorption of $S_2O_8^{2-}$ occurs, thus leading to a negative shift of the electrode potential (E) to promote the SO_4^{2-} desorption and keep a constant current density (j). The negative shift in E, in turn, leads to a decrease in θ_{OH} and hence a decrease in k_{1a} ($=k_{1a0} + \theta_{OH}$), which leads to a further negative shift in E to keep a constant j. Here is a positive feedback mechanism, and this causes a transition to a low-potential state.

In a low-potential state, the desorption of adsorbed SO_4^{2-} becomes fast, which leads to an increase in vacant surface sites for the $S_2O_8^{2-}$ reduction and to a positive shift in E. The positive shift in E leads to an increase in θ_{OH} and k_{1a} and to a further positive shift in E to keep a constant j. Here is also a positive feedback mechanism, which leads to a transition to a high-potential state.

The NDR observed for the $S_2O_8^{2-}$ reduction strongly depends on the crystal faces of single-crystal Au electrodes and the atomic flatness at the surface (Figure 6). The NDR arising from the autocatalytic effect of adsorbed OH in the H_2O_2-reduction system showed quite the same behavior,[17] as already mentioned. We can assume that the dissociative adsorption of negatively charged $S_2O_8^{2-}$ occurs rapidly on positively polarized metal atoms in the neighborhood of adsorbed OH (Figure 10), similar to the case of dissociative adsorption of H_2O_2.[17] The difference in the ζ value in eq 3 among crystal faces of Au electrodes can be attributed to the difference in the number of the positively polarized metal atoms around adsorbed OH, as reported.[17,19]

Finally, let us consider briefly oscillations other than oscillation γ. Oscillation α is of a character similar to oscillation A in the H_2O_2-reduction system, as mentioned before. This implies that the NDR for oscillation α arises from the suppression of the $S_2O_8^{2-}$ reduction by the formation of upd-H. However, a question remains on how the upd-H suppresses the $S_2O_8^{2-}$ reduction, because, in a potential region of oscillation α, the $S_2O_8^{2-}$ reduction is reported to proceed via no adsorption.[31] For oscillations β and δ, impedance measurements revealed that they were of an HNDR-type, though further details are unclear at present. In solutions of high ionic strengths in this work, oscillations due to the Frumkin effect[26,27] are not observed. On the other hand, oscillations α, β, γ, and δ will in principle be observed in solutions of low ionic strengths, though the appearance of oscillations depends on detailed conditions in various factors. In fact, oscillation α is observed even in 1.0 mM $Na_2S_2O_8$.

In conclusion, this work has revealed that the $S_2O_8^{2-}$ reduction on Pt and Au in high ionic strength electrolytes shows four oscillations of different kinds, named oscillations α, β, γ, and δ. Detailed studies on oscillation γ showed that adsorbed

OH has a catalytic effect on the dissociative adsorption of $S_2O_8^{2-}$, leading to the appearance of oscillation γ. The present results as well as the reported ones on the H_2O_2 reduction[17,19] show the generality of an autocatalytic (or a catalytic) effect of adsorbed OH on electrochemical reactions.

References and Notes

(1) Hudson, J. L.; Tsotsis, T. T. *Chem. Eng. Sci.* **1994**, *49*, 1493.

(2) Fahidy, T. Z.; Gu, Z. H. *Modern Aspects of Electrochemistry*; White, R. E., Bockris, J. O'M., Conway, R. E., Eds.; Plenum: New York, 1995; Vol. 27, p 383.

(3) Koper, M. T. M. *Advances in Chemical Physics*; Prigogine, I., Rice, S. A., Eds.; John Willey & Sons: New York, 1996; Vol. 92; p 161.

(4) Krischer, K. *Modern Aspects of Electrochemistry*; White, R. E., Bockris, J. O'M., Conway, R. E., Eds.; Plenum: New York, 1999; Vol. 32, p 1.

(5) Strasser, P.; Eiswirth, M.; Koper, M. T. M. *J. Electroanal. Chem.* **1999**, *478*, 50.

(6) Flätgen, G.; Krischer, K.; Pettinger, B.; Doblhofer, K.; Junkes, H.; Ertl, G. *Science* **1995**, *269*, 668.

(7) Kiss, I. Z.; Gaspar, V.; Hudson, J. L. *J. Phys. Chem. B* **2000**, *104*, 7554.

(8) Christoph, J.; Otterstedt, R. D.; Eiswirth, M.; Jaeger, N. I.; Hudson, J. L. *J. Chem. Phys.* **1999**, *110*, 8614.

(9) Strasser, P.; Christoph, J.; Lin, W. F.; Eiswirth, M.; Hudson, J. L. *J. Phys. Chem. A* **2000**, *104*, 1854.

(10) Mazouz, N.; Krischer, K.; Flätgen, G.; Ertl, G. *J. Phys. Chem. B* **1997**, *101*, 2403.

(11) Li, Y. J.; Oslonovitch, J.; Mazouz, N.; Plenge, F.; Krischer, K.; Ertl, G. *Science* **2001**, *291*, 2395.

(12) Mukouyama, Y.; Nakanishi, S.; Nakato, Y. *Bull. Chem. Soc. Jpn.* **1999**, *72*, 25736.

(13) Matsuda, T.; Hommura, H.; Mukouyama, Y.; Yae, S.; Nakato, Y. *J. Electrochem. Soc.* **1997**, *144*, 1988.

(14) Mukouyama, Y.; Nakanishi, S.; Konishi, H.; Nakato, Y. *J. Electroanal. Chem.* **1999**, *473*, 156.

(15) Mukouyama, Y.; Nakanishi, S.; Chiba, T.; Murakoshi, K.; Nakato, Y. *J. Phys. Chem. B* **2001**, *105*, 7246.

(16) Mukouyama, Y.; Nakanishi, S.; Konishi, H.; Ikeshima, Y.; Nakato, Y. *J. Phys. Chem. B* **2001**, *105*, 10905.

(17) Nakanishi, S.; Mukouayma, Y.; Karasumi, K.; Imanishi, A.; Furuya, N.; Nakato, Y. *J. Phys. Chem. B* **2000**, *104*, 4181.

(18) Nakanishi, S.; Mukouayama, Y.; Nakato, Y. *J. Electrochem. Soc.* **2001**, *148*, E405.

(19) Nakanishi, S.; Mukouyama, Y.; Nakato, Y. *J. Phys. Chem. B* **2001**, *105*, 5751.

(20) Flätgen, G.; Wasle, S.; Lübke, M.; Eickes, C.; Radhakirishnan, G.; Doblhofer, K.; Ertl, G. *Electrochim. Acta* **1999**, *44*, 4499.

(21) Frumkin, A. N. *Z. Electrochem.* **1955**, *59*, 807.

(22) Gokhshtein, A. Y.; Frumkin, A. N. *Dokl. Akad. Nauk. SSSR* **1960**, *132*, 388.

(23) Frumkin, A. N.; Petti, O. A.; Nikolaeva-Fedorovich, N. V. *Dokl. Akad. Nauk. SSSR* **1961**, *136*, 1158.

(24) Koper, M. T. M. *Ber. Bunsen-Ges. Phys. Chem.* **1996**, *424*, 497.

(25) Flätgen, G.; Krischer, K.; Ertl, G. *J. Electroanal. Chem.* **1996**, *409*, 183.

(26) Treindl, L.; Doblhofer, K.; Krischer, K.; Samec, Z. *Electrochim. Acta* **1999**, *44*, 3963.

(27) Wolf, W.; Ye, J.; Purgand, M.; Eiswirth, M.; Doblhofer, K. *Ber. Bunsen-Ges. Phys. Chem.* **1992**, *96*, 278.

(28) Clavilier, J.; Faure, R.; Guinet, G.; Durand, D. *J. Electrochem. Soc.* **1980**, *107*, 205.

(29) Müller, L. *J. Electroanal. Chem.* **1967**, *13*, 275.

(30) Müller, L.; Wetzel, W.; Otto, H. *J. Electroanal. Chem.* **1970**, *24*, 175.

(31) Samec, Z.; Doblhofer, K. *J. Electroanal. Chem.* **1994**, *367*, 141.

(32) Zelin, L.; Tinghua, W.; Ke, C. *Chin. J. Chem. Phys.* **1999**, *12*, 251 (in Chinese).

(33) Itaya, K.; Sugawara, S.; Sashikata, K.; Furuya, N. *J. Vac. Sci. Technol.* **1990**, *A8* (1), 515.

(34) Desilvestro, J.; Weaver, M. J. *J. Electroanal. Chem.* **1987**, *234*, 237.